Desalination and Water Treatment
www.deswater.com

doi: 10.5004/dwt.2021.27646

239 (2021) 202–216
November

Mathematical approach to artificial neural network on Methyl violet removal with magnetically coated activated carbon

Esra Altıntığ[a], Selma Altundag[b], Iknur Yakan[c], Dilay Bozdag[d], Huseyin Altundag[c,*]

[a]*Sakarya University of Applied Sciences, Pamukova Vocational School, 54055 Sakarya, Turkey, email: altintig@subu.edu.tr*
[b]*Department of Mathematics, Faculty of Arts and Sciences, Sakarya University, 54187 Sakarya, Turkey, email: scaylan@sakarya.edu.tr*
[c]*Department of Chemistry, Faculty of Arts and Sciences, Sakarya University, 54187 Sakarya, Turkey, email: altundag@sakarya.edu.tr (H. Altundag), ilkr.yakan@gmail.com (I. Yakan)*
[d]*Department of Industrial Engineering, Faculty of Engineering, Sakarya University, 54187 Sakarya, Turkey, email: dilay.bozdag1@ogr.sakarya.edu.tr*

Received 27 April 2021; Accepted 22 July 2021

ABSTRACT

In this study, new magnetic activated carbon (Fe_3O_4-AC) was synthesized from activated carbon which was obtained from the inner bark of acorn with the activation of H_3PO_4 and its effectiveness in Methyl violet (MV) removal from aqueous solutions was investigated. Characterization of the samples was done by scanning electron microscopy–energy-dispersive X-ray spectroscopy, X-ray diffraction and Fourier-transform infrared spectroscopy. In MV adsorption on Fe_3O_4-AC, pH (2–10), initial MV concentration (25–150 mg/L), amount of adsorbent (0.1–1.0 g), adsorption time (5–180 min) and temperature (298–318 K) adsorption parameters were investigated. The compatibility of MV and Fe_3O_4-AC adsorption with Langmuir and Freundlich isotherm models was investigated, and it was determined that Langmuir isotherm which proposed single-layer adsorption, was the most compatible isotherm for adsorption at three different temperatures. The highest maximum adsorption capacity with Langmuir isotherm was obtained as 156.25 mg/g at 298 K. The pseudo-second-order kinetic model had a better fit with the best correlation to the kinetic data. Thermodynamic parameters ($\Delta G°$, $\Delta H°$ and $\Delta S°$) were calculated from the Van't Hoff plot of $\ln K_d$. $1/T$ in order to discuss the removal mechanism of MV. Then, in MV removal process under different conditions, experimental results were compared with the artificial neural network model.

Keywords: Adsorption; Dye removal; Methyl violet; Artificial neural network; Activated carbon

1. Introduction

With the rapidly increasing population in the world and our country, problems arise in many areas. Dyestuff is widely used in industries such as textile, paper, cosmetics, leather and food. Extensive use of dyes generates cloudy wastewater that causes serious damage to the ecosystem [1]. However, the complex aromatic molecular structures of dyes make them more stable and make it difficult to biodegrade from wastewater. It is very important to remove these dyestuffs from wastewater. Therefore, the removal of these polluting ions is extremely important for the protection of human life and the environment [2–4]. For this purpose, coagulation-flocculation, adsorption, precipitation and oxidation methods were developed to remove dye contaminants from industrial wastes [5]. The adsorption method is the most preferred among various chemical and biological methods for cleaning polluted waters due to its high performance, economic applicability, suitability in a wide concentration range, ease of installation and low energy

* Corresponding author.

consumption [6]. The cost of the adsorption technique depends on the price of the adsorbent [7]. Therefore, many scientists are working on low-cost adsorbent production from agricultural wastes [8]. Activated carbons are useful products that do not harm human health and nature and have very high porosity and internal surface area which activated carbon can attract molecules and ions in the solution through their pores towards their inner surfaces and therefore called adsorbents [9]. They have a variety of engineering surface groups that can be used in many specific applications, including purification, chlorine reduction, toxicity reduction, separability and concentration of recoverable materials [2,9]. Although activated carbons are frequently used in adsorption processes, it is difficult to remove small size particles from aqueous solutions [10]. In order to increase the adsorption capacity of adsorbents for the removal of dye, various modification materials and methods have been used; such as cationic surfactants [11], magnetic particles [12], metal oxides [13], chemical activating agents [14]. For this reason, the number of studies on the magnetic properties of AC has been increasing recently. Magnetically AC can be separated from the environment by magnet or external magnetic field [15]. In addition to the use of activated carbon for dye treatment, the magnetic activated carbon nanoparticles can be modified due to reusability and due to their high surface area, they are used for the removal of organic contaminants from aqueous solutions [16]. In recent years, the magnetic property of activated carbon has been used to assist other methods. Gaining magnetic properties to activated carbons by precipitation of Fe^{2+} and Fe^{3+} salts has become one of the most preferred methods in recent years due to its ease of application and more results that are efficient are obtained. In addition, the preparation of magnetized materials requires special chemicals and procedures that must be followed in several steps. Due to its low production cost, easy preparation of superparamagnetic magnetite (Fe_3O_4) nanoparticles, good biocompatibility, and no contaminants, it is preferred to be used in dye adsorption by modifying with ACs [17,18]. For this purpose, magnetic composites with high surface area and high adsorption capacity based on activated carbon/iron oxide and clay/iron oxide have been developed to remove contaminants from aqueous surfaces [19].

Artificial neural networks are now commonly used in many areas of chemistry. Artificial neural networks, one of the features of based modeling do not require mathematical knowledge. Therefore, description of events in the process and is a useful method for simulation and scaling of complex adsorption systems [20,21]. Due to the various reactions during the adsorption process and interactions occur. Lack of knowledge about reactions and the complexity of the process can be solved by artificial neural networks (ANN) modeling using black-box methods [22]. In the literature, usually, the hidden layer and the number of processing elements in these layers are determined by the trial-and-error method [23]. There is no rule for determining the number of hidden (intermediate) layers and the number of processing elements in hidden layers. Therefore, when the valid mathematical model is unknown, ANN is a versatile and highly flexible method used to model complex relationships between variables [24].

In this study, AC was produced from acorn shells, which coated with Fe_3O_4 magnetite nanoparticles by co-precipitation method in order to increase the adsorption capacity. Samples before and after adsorption were characterized by analytical methods such as Fourier-transform infrared spectroscopy (FTIR), X-ray diffraction (XRD), SEM and scanning electron microscopy–energy-dispersive X-ray spectroscopy. To determine the adsorption of Fe_3O_4-AC on the Methyl violet (MV), pH value, adsorbent dosage, temperature, contact time and initial concentration of the solution were investigated. Adsorption isotherms, thermodynamic and kinetic studies were also carried out, and the adsorption mechanism was revealed. Adsorption-desorption experiments and adsorbent reusability were investigated. In addition to these studies, the usability of Fe_3O_4/AC as an adsorbent in removing MV from a solution medium has been investigated and an ANN model is presented by considering the effect of experimental parameters on MV adsorption.

2. Materials and methods

2.1. Material

Analytical grade chemicals NaOH, HCl, cationic dye (MV), $FeSO_4{\cdot}7H_2O$ and $FeCl_3{\cdot}6H_2O$ were purchased from Merck Company (Germany). All chemicals used in the study are analytical grade. In this study, the inner shell of the acorn used to obtain AC was collected from Sakarya Turkey. The acorn used to remove the pollution in the wastewater was washed once with distilled water. The washed acorn was dried in the oven at 378 K for 24 h. The dried sample was shredded by mortar and sieved until the shells were smaller than 4 mm. The mixing of the chemicals was done using an IKA KS 501 orbital shaker. A METTLER TOLEDO pH meter was used for pH measurement of the solutions and a BLULAB drying chamber for drying processes. The disintegrated shells were kept free from air contact.

2.2. Preparation of AC adsorbent

The preparation of the AC adsorbent was carried out in two steps in the present study: chemical activation and characterization. H_3PO_4 was used for chemical activation. First of all, the activation process was made by mixing the inner shells of acorn with H_3PO_4 at a ratio of 1/3. It was then carbonized under nitrogen gas flow (150 cm^3/min) for 1 h at 700°C. Acorn inner shells were mixed in a magnetic stirrer at 70°C for 2 h so that the acid could be in good contact, and then filtered. The filtered samples were allowed to dry for 24 h without exceeding 100°C.

2.3. Preparation of Fe_3O_4-AC adsorbent

First, a solution of $FeSO_4{\cdot}7H_2O$ (3.75 g, 14 mmol) and $FeCl_3$ (0.7 g, 14 mmol) was added to a 500 mL beaker and heated at 353 K. 6.25 g of AC was weighed and added to the mixture. 100 mL of 5 mol/L NaOH was added dropwise for 5 min to adjust the pH to 10 and Fe_3O_4 in the mixture precipitated. The magnetic property of the black precipitate formed while changing the color of the prepared composite was determined by the orientation of the whole precipitate towards the magnet when the neodymium

magnet was brought closer to the beaker containing the solution. Nitrogen gas was continued to be introduced into the solution during the stirring time. The resulting magnetic adsorbent was washed with distilled deionized water and filtered with blue band filter paper. Finally, the magnetic adsorbent was dried in an oven at 353 K for 2 h. The synthesis schema of the Fe_3O_4-AC adsorbent is illustrated in Fig. 1.

2.4. Analytical measurements

SEM analysis was performed with JEOL JSM-6060 LV model device to investigate surface images of acorn inner bark, AC, before adsorption Fe_3O_4-AC and after adsorption Fe_3O_4-AC samples under different conditions. To ensure conductivity, the powder was coated with Au, which is used in SEM analysis, at a thickness of 2 nm.

Structural analyzes of acorn inner bark, AC, before adsorption Fe_3O_4-AC and after adsorption Fe_3O_4-AC samples were performed with (Rigaku) brand XRD device.

The main functional groups of bonito inner bark, AC, Fe_3O_4-AC before adsorption and Fe_3O_4-AC samples after adsorption were characterized using FTIR device. In the Shimadzu model device, the functional group adsorbent values between the range of 600 and 4,000 cm^{-1} and the structure were tried to be illuminated by the ATR method. FTIR the vibrational motions of molecules were bound to the surface by infrared rays.

2.5. Adsorption experiments

The MV stock solution was prepared at a concentration of 1,000 mg/L. Standard solutions (1–10 mg/L) and working solutions (25–150 mg/L) were prepared from stock solutions by diluting with deionized water (chemical resistance: 18 MΩ cm).

0.1 M NaOH or 0.1 M HCl were used to adjust the pH of the adsorption assay solutions. In the experiment, 100 mL dyed solution was used to remove dyestuffs from water solutions. Adsorbent dosage (0.1–1.0 g), pH (2–10), dye concentration (25–150 mg/L) and process temperature were maintained at 298–318 K and at constant contact time intervals in the water bath shaker at 120 rpm (5–180 min). The dye concentration was determined in UV spectrometer at 579 nm. Adsorption experiments performed in different parameters were repeated 3 times and average values were presented.

The amounts of solutions obtained for dye removal were calculated using the following mathematical equations:

$$q_e = \frac{\left(C_o - C_e\right)}{m} \times V \tag{1}$$

$$\text{Removal}\left(\%\right) = \frac{\left(C_o - C_e\right)}{C_o} \times 100 \tag{2}$$

where q_e is the adsorption capacity of dye (mg/g), C_o is the initial dyestuff (MV) concentration (mg/L), C_e is the final concentration of MV (mg/L), V is the solution volume (mL), m is the weight of the adsorbent (g).

2.6. Desorption and regeneration studies

The desorption process of the activated carbon synthesized using H_3PO_4 was carried out for the recovery of the adsorbent obtained at different temperatures and different impregnation by giving the magnetic property [25]. In this study, desorption was carried out with 0.1–0.5 M NaOH (50 mL). Magnetic nanoparticles (0.1–0.5 g) impregnated with methyl viol were placed on desorption medium and shaken at 120 rpm for 1 h on a rotary shaker. The best result achieved was a cycle study. The adsorbent was separated and rinsed with distilled water. The amount of desorption (%D) was calculated according to Eq. (3).

$$\text{Desorption}\left(D\%\right) = \frac{C_d}{C_a} \times 100 \tag{3}$$

where C_a (mg/g) is the amount adsorbed, and C_d (mg/g) is the amount of desorption.

2.7. Modeling studies with artificial neural networks

In the input layer of the ANN model developed for MV adsorption experiments, there are 5 process elements containing information on adsorbate concentration, initial pH, temperature, adsorbent amount and contact time, and 1 processing element containing data on percent adsorption in the output layer. In this study, the toolbox named Neural Fitting Tool in MATLAB 2008a version was used to

Fig. 1. The synthesis schema of the Fe_3O_4-AC adsorbent.

create the ANN model which uses one hidden layer and the number of neurons in this hidden layer can be changed. The trial-and-error method used in the literature was used to determine the number of neurons. The sigmoid transfer function (tansig) is used in the hidden layer and the linear transfer function (purelin) is used in the output layer. The input matrix [G] and output vector {C} are formed from the data obtained from the experiments. Input and output data are introduced to the network using the normalization technique. Eq. (4) has been used in scaling (normalizing) inputs and outputs [26].

$$A_i = 0.8\left[\frac{X_i - \min(X_i)}{\max(X_i) - \min(X_i)}\right] + 0.1 \quad (4)$$

In this equation, x' means normalized value, x_i is the real value, x_{min} is the smallest value, x_{max} is the largest value. Neural network is used to process both linear and non-linear processes is used to find the relationship between input and output targets.

3. Results and discussions

3.1. Characterization results of adsorbents

Important data are obtained with XRD about the composition of the inorganic material in the structure. Fig. 5 shows the XRD results of (a) acorn inner shells, (b) AC, (c) Fe_3O_4-AC before adsorption and (d) Fe_3O_4-AC after adsorption.

In the XRD spectrum of the acorn inner bark sample shown in Fig. 2a, the peaks are 18.46°, 25.18° and 39.01°. These peaks are due to the carbon in the structure. Despite the shifts observed in these peaks with the conversion of the structure to activated carbon, a similar structure is seen when compared to the AC in Fig. 2b. Both samples are amorphous. Similar results are seen in the literature [9,27,28]. The characteristic 30.02° (220), 35.73° (311), 43.25° (400), 57.60° (511), 63.39° (440) 2θ peaks observed in Fig. 2c belong to Fe_3O_4 [27,28]. In our study, these sharp peaks were observed after AC magnetization. In Fig. 2d, it was seen that the intensity of these peaks observed after MV adsorption decreased after adsorption.

Fig. 3 shows the results of the FTIR analysis of the samples obtained as a result of (a) acorn inner shells, (b) AC, (c) Fe_3O_4-AC before adsorption and (d) Fe_3O_4-AC after adsorption

The band observed around 3,500 cm^{-1} in Fig. 3a corresponds to the stress vibration of the $[OH]^-$ groups. This peak Fig. 3b–d has disappeared. This is due to the high temperature used in activation [29]. The peak observed at 1,648 cm^{-1} in Fig. 3a belongs to the C=O stretching vibration. In addition, the weak peak observed at 1,490 cm^{-1} is due to aliphatic CH_2 bending vibration and CH_3 bending vibration [30]. 1,024 cm^{-1} shows the peak alcohol groups (ROH). C–OH and O–H stress is observed in alcohol and phenol groups at 1,100 cm^{-1}. The peaks seen at 500–750 cm^{-1} in Fig. 3c and d correspond to the stretching vibration due to the interactions of Fe–O–Fe in the Fe_3O_4 [31]. Aliphatic ether C–O and ester C–O strain are observed at 1,150 cm^{-1}. It indicates that AC has a high surface area and ability to hold other metals [32].

Fig. 4 shows SEM photographs of the (a) acorn inner shells, (b) AC, (c) Fe_3O_4-AC before adsorption and (d) Fe_3O_4-AC after adsorption samples. Acorn inner shells surface has a porous structure. Since AC has a porous structure prior to activation process, when SEM image is examined, it is thought that the gaps on the surface were

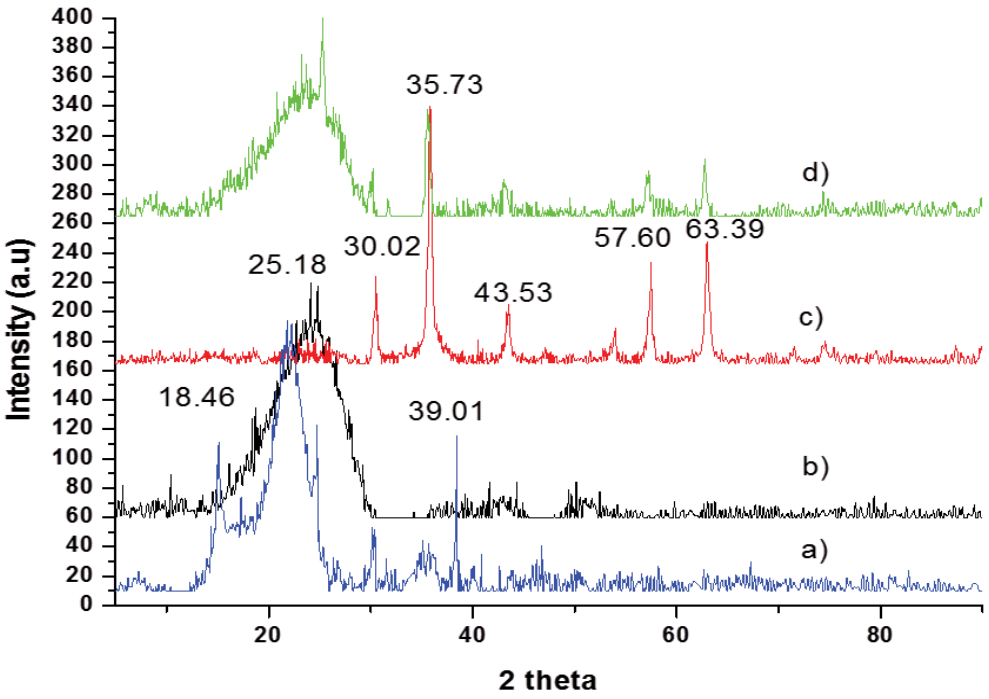

Fig. 2. XRD patterns of (a) acorn shell, (b) AC, (c) Fe_3O_4-AC, and (d) Fe_3O_4-AC after adsorption.

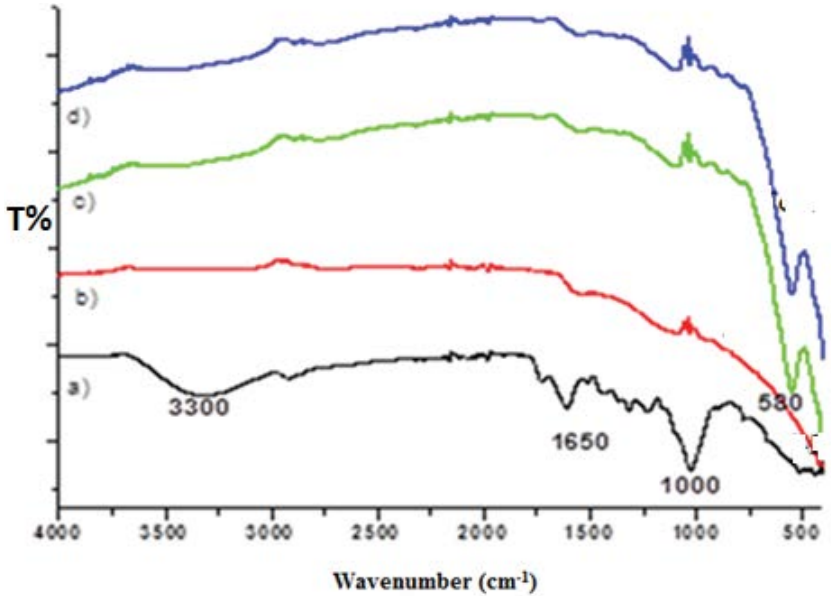

Fig. 3. FTIR spectrum of (a) acorn shell, (b) AC, (c) Fe_3O_4-AC, and (d) Fe_3O_4-AC after adsorption.

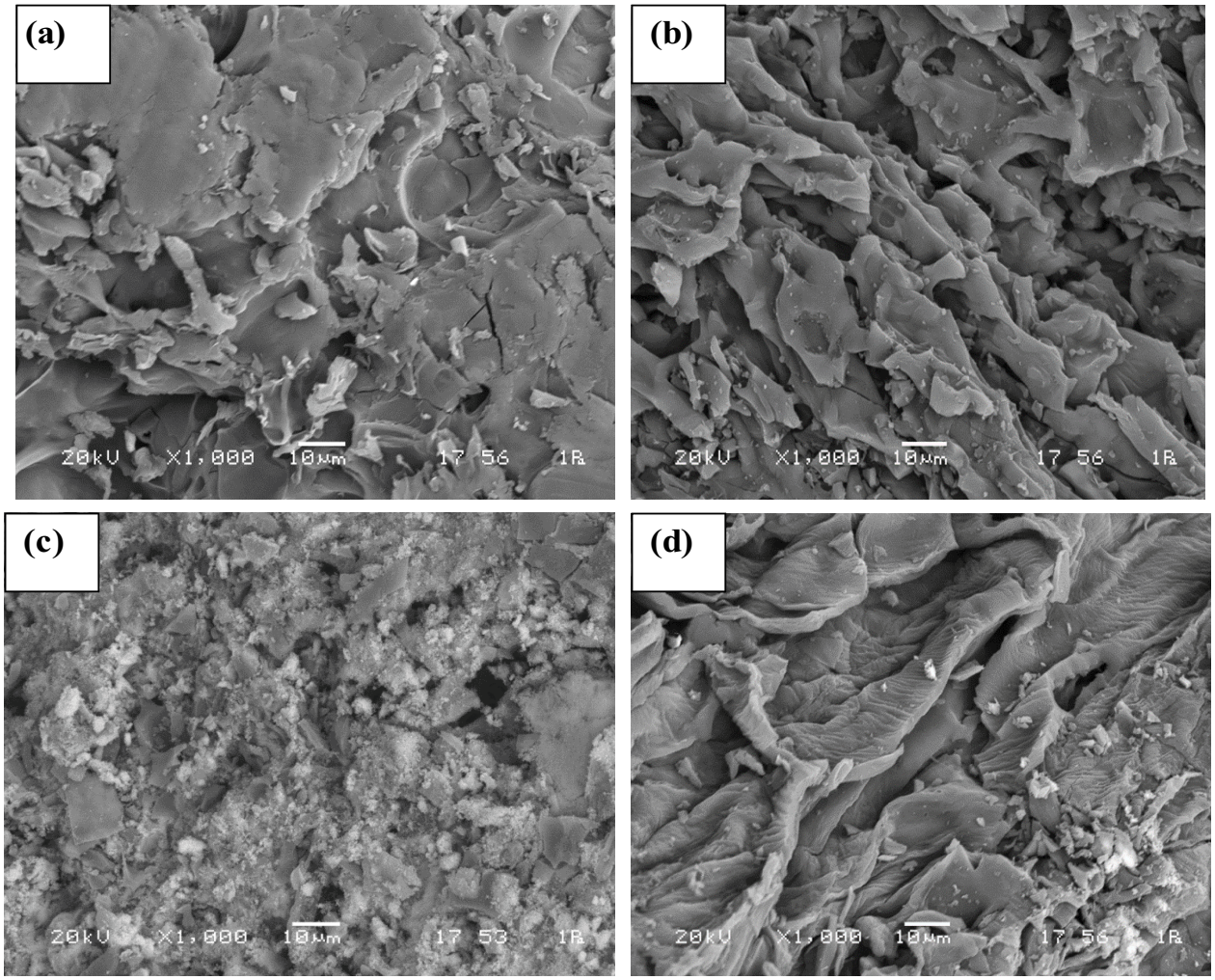

Fig. 4. SEM photographs of (a) acorn shell, (b) AC, (c) Fe_3O_4-AC and (d) Fe_3O_4-AC after adsorption.

filled by the chemical reagent beforehand and that these gaps were formed on the surface of the activated carbon by evaporation of the chemical substance during carbonization (a and b) [33,34]. When Fe_3O_4 loading takes place on the AC, it is observed that the recesses and protrusions on the AC are partially interfered with the particles of nanoscale and the particles are retained on the surface. It is observed that MV is attached to the porous surface of the Fe_3O_4-AC and inside the crevices, while its surface has a more homogeneous appearance (c and d). As a result, small particle size, large surface area and porous adsorbents increase the adsorption capacity.

As can be seen from the energy-dispersive X-ray spectroscopy (EDS) results in Fig. 5, element C is due to AC being the main component of the adsorbent. Fe and O are formed as a result of coating the structure with Fe_3O_4. This result is proof that the adsorbent we obtained is composed of C, Fe and O. The P component depends on the H_3PO_4 used for activation of the adsorbent. In the EDS map of the element Fe, it is observed that nano-sized magnetite particles are homogeneously distributed and covered on the Fe_3O_4-AC adsorbent surface. Si observed in the analysis comes from soil.

3.2. Effect of pH on the MV adsorption

Solution pH is one of the most important parameters affecting the removal process of dyestuffs. By influencing the material's surface charge, degree of ionization, and molecules or iron speciation affects the process [35,36]. To investigate the effect of pH on the adsorption of MV by Fe_3O_4-AC, MV solutions were prepared at varying pH (2–10) and concentration of 50, 100 and 150 mg/L. Data on the effect of initial pH on MV adsorption are shown in Fig. 6.

When Fig. 6 was examined, it was observed that MV adsorption increased from pH 2 to pH 4 for three different concentrations, while it stabilized after pH 4. The highest yield was found to be associated with pH 6. At this pH, the adsorption efficiency was calculated as 97.59%, 96.71% and 94.12% at 50, 100 and 150 mg/L MV concentrations, respectively. A slight decrease in yield was observed as the concentration increased. The results show that the pH of

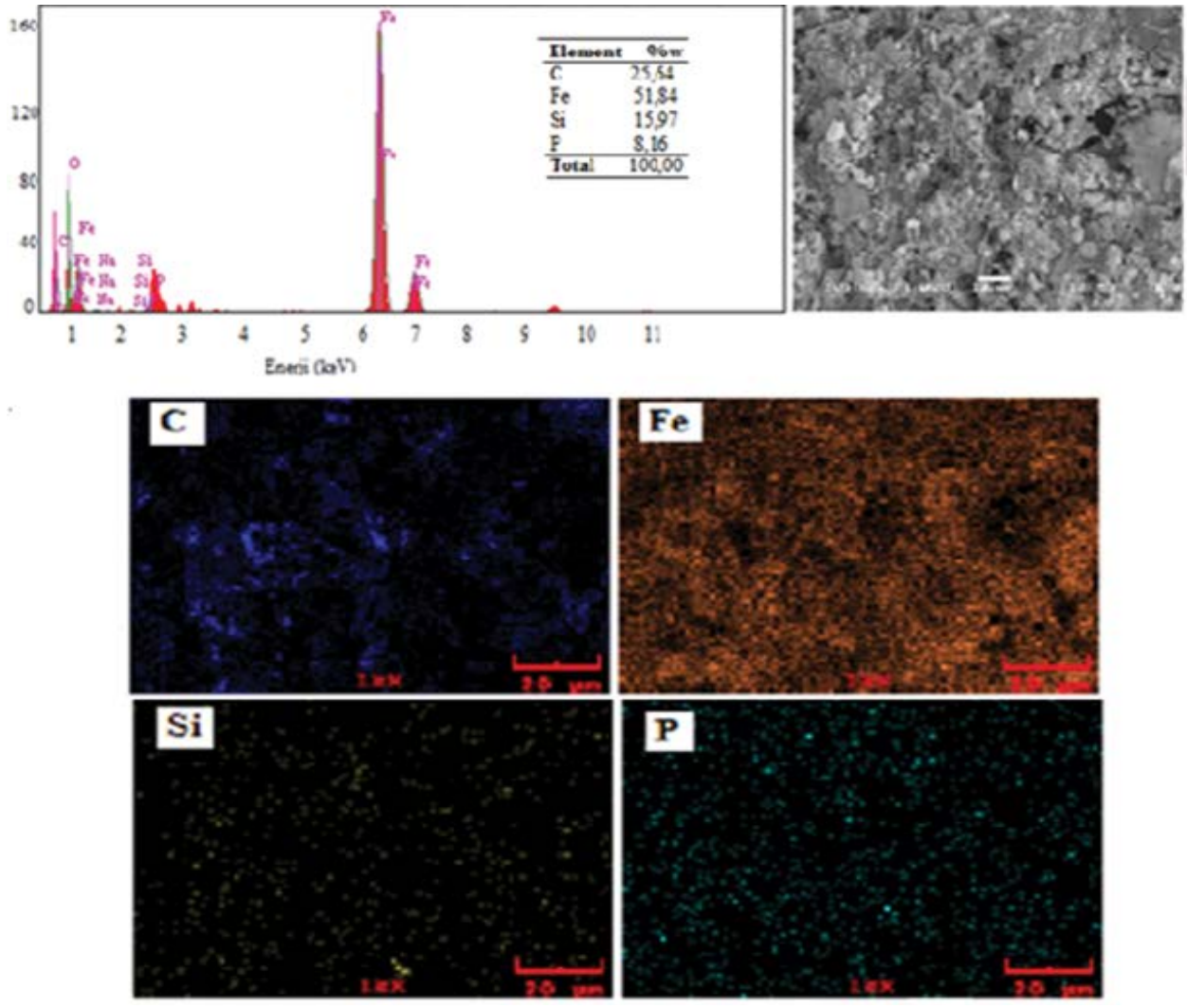

Fig. 5. SEM/EDS results were obtained for the Fe_3O_4-AC sorbents.

the solution seems to be an important factor in influencing the adsorption. Thus, pH 6.0 was chosen as the optimum pH value and used for all subsequent experiments. There are similar results in the literature [25,35,36].

3.3. Effect of contact time on the adsorption efficiency

The values obtained as a result of from the experiments show that the characteristics of the material attached to the adsorbent surface have the effect of balancing the adsorption time [37]. The effect of contact time on MV adsorption on Fe_3O_4-AC was investigated at 50, 100 and 150 mg/L MV concentrations, respectively, for periods ranging from 5 to 180 min. The effect of contact time on Fe_3O_4-AC MV adsorption is shown in Fig. 7.

In Fig. 7, it was observed that MV adsorption increased and remained constant up to 120 min. The MV adsorption equilibrium time was found to be 120 min. From the results of the experiments, it was seen that the properties of the substance, the nature of the adsorbent and the exchangeable sorption centers of the adsorbent all affect the equilibrium time of the adsorption process.

3.4. Adsorbent dose effect on MV removal yield

Adsorbent dose is one of the reasons affecting the removal efficiency. If the adsorbent dose is insufficient, the maximum removal efficiency may decrease, otherwise, if it is high, flocculation may occur in the solution. Both situations adversely affect adsorption [38]. In this study, the

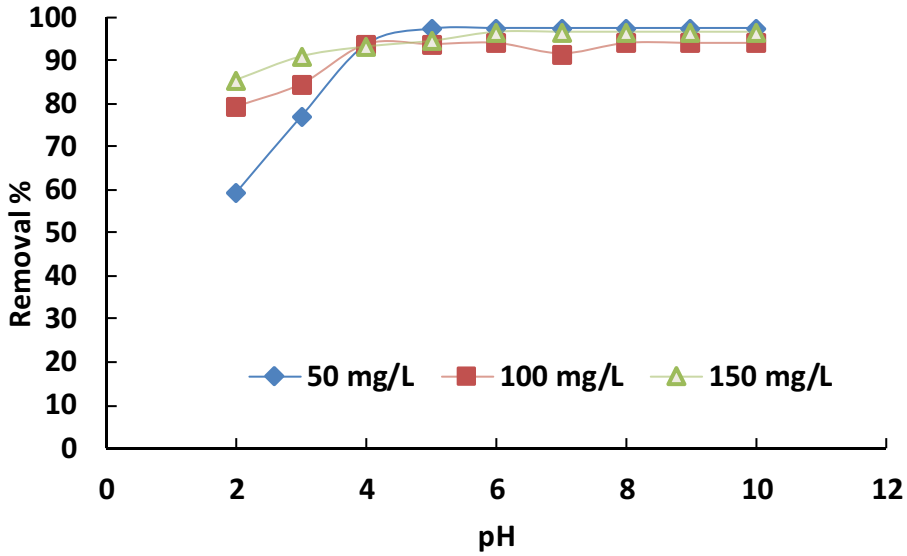

Fig. 6. Effect of pH on the MV adsorption (MV concentration: 50, 100 and 150 mg/L; temperature: 298 K; adsorbent dosage: 0.1 g).

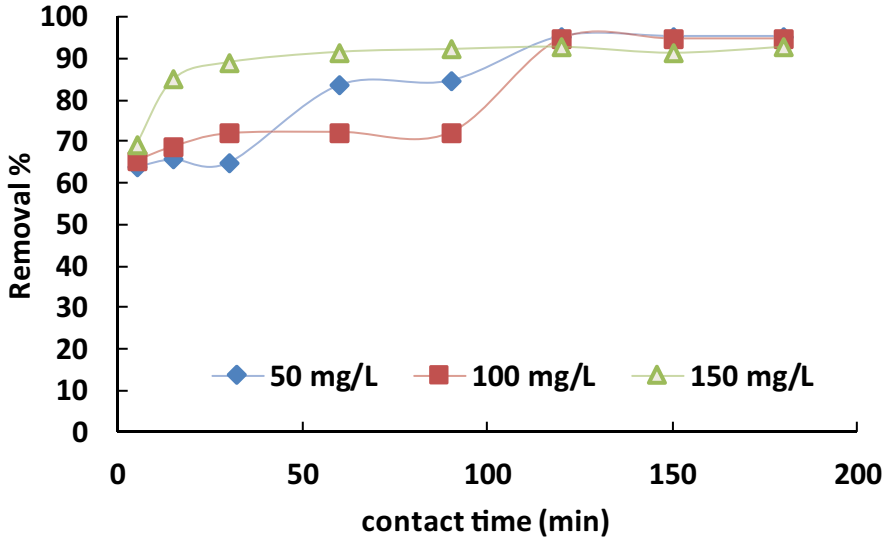

Fig. 7. Effect of contact time on the adsorption of MV (MV concentration: 50, 100 and 150 mg/L; temperature: 298 K; pH = 6.0; adsorbent dosage: 0.1 g).

adsorbent dose was calculated between 0.1–1.0 g/100 mL and at three different MV concentrations, pH 6 and 298 K (Fig. 8).

Fig. 8 shows the effect of adsorbent dose on MV removal efficiency. When the graph is examined, it is observed that the removal efficiency is over 95% when 0.1 g adsorbent dose is used in all three concentrations, while the removal efficiency decreases when the adsorbent dose is increased. Based on these results, we continued our other studies with an optimum adsorbent dose of 0.1 g.

3.5. Adsorption isotherms

The equilibrium data were modeled using Langmuir and Freundlich isotherm equations to determine the type of adsorption and to determine the maximum removal capacity of the adsorbent developed for MV removal. Langmuir isotherm is the most widely used isotherm in terms of theoretical adsorption of contaminants from liquid solutions. It is valid for single layer adsorption of certain homogeneous areas and pollutants [39]. The Freundlich isotherm is the first equation that describes the adsorption process. In the empirical equation, this isotherm is used to describe the properties of a heterogeneous system. This isotherm assumes that the adsorbed enthalpy decreases logarithmically by the occupied area. Freundlich isotherm is recommended for heterogeneous surfaces [39]. In this study, Freundlich and Langmuir adsorption isotherms were used to analyze the experimental data. The applicability of isotherm equations to experimental data was evaluated using correlation coefficients [40].

When the equilibrium is reached, the analysis of adsorption data is important for the optimization of the adsorption process. Using the data obtained from different studies, it was investigated with the help of different adsorption isotherms (Langmuir and Freundlich isotherms).

To investigate the MV adsorption isotherms of the Fe_3O_4-AC adsorbent, Langmuir equation is shown as in Eq. (5):

$$q_e = \frac{K_L q_m C_e}{1 + K_L C_e} \tag{5}$$

In this equation: q_m is the maximum adsorption capacity (mg/g), K_L is the Langmuir constant, C_e is the concentration of adsorbate (mg/L) in solution at equilibrium [41].

The Freundlich isotherm is an empirical equation that can be used for heterogeneous systems for with interactions between adsorbed molecules [42]. The formula of the model is shown in Eq. (6).

$$\log q_e = \log K_f + \frac{1}{n} \log C_e \tag{6}$$

where K_f (L/g); a constant fixed by adsorption capacity $1/n$; a model parameter including adsorption intensity, n; adsorption intensity.

Linear graphs of Langmuir and Freundlich adsorption isotherms for 3 different temperatures are shown in Figs. 9–10 and the results obtained from the isotherm models are presented in Table 1.

When we look at the R^2 values in the adsorption process in Table 1, values close to 1 show that adsorption is more suitable for the Langmuir isotherm. Compliance with the Langmuir equation is the result of a monolayer adsorption. From the Langmuir equation, the highest maximum adsorption capacity (q_{max}) was calculated as 156.25 mg/g at 278 K, 155.84 mg/g at 308 K and 136.98 mg/g at 318 K, respectively. In addition, when Table 1 is examined, q_{max} decreases as the temperature increases. These results show us that Fe_3O_4-AC is more successful in low temperature dyestuff removal.

3.6. Adsorption thermodynamics

One of the important parameters to determine the thermal properties of the adsorption process is temperature.

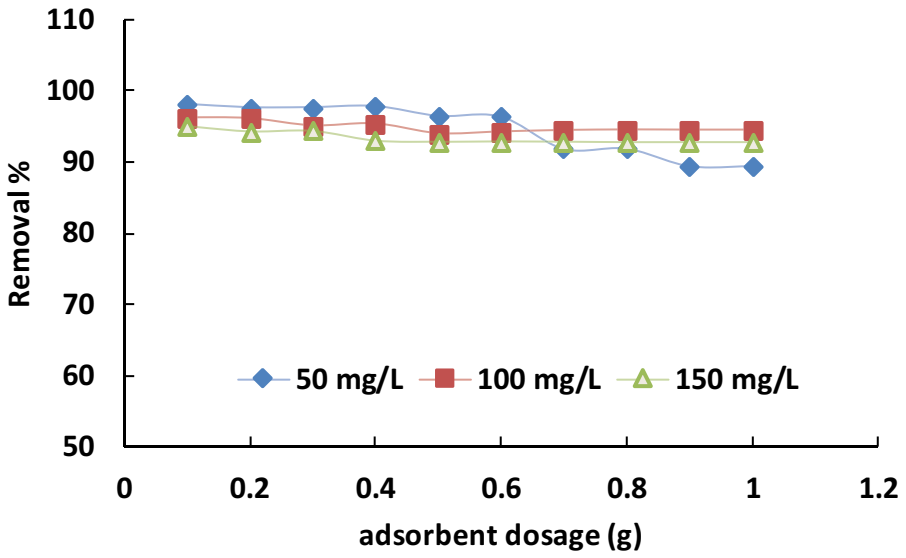

Fig. 8. Effect of adsorbent dosage on the adsorption of MV (MV initial concentration: 50, 100 and 150 mg/L; temperature: 298 K; contact time: 120 min).

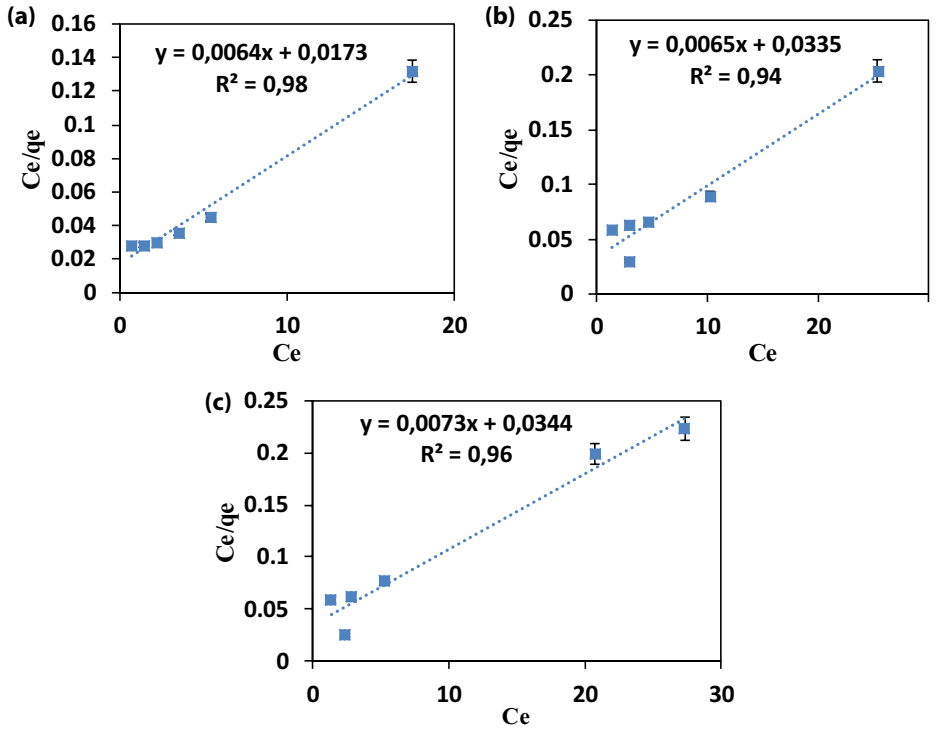

Fig. 9. Langmuir isotherm plots were obtained for the adsorption MV onto Fe_3O_4-AC sorbent (a) 298 K, (b) 308 K and (c) 318 K (pH: 6.0; contact time: 120 min; adsorbent dose: 0.1 g).

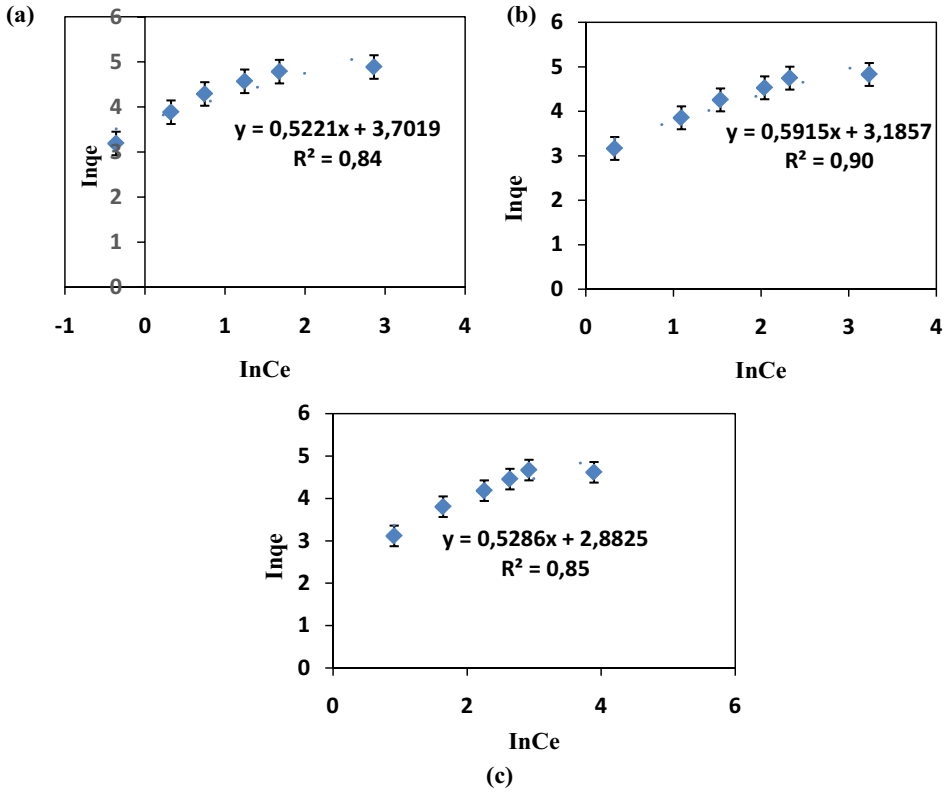

Fig. 10. Freundlich plots obtained for the adsorption MV onto Fe_3O_4-AC sorbent (a) 298 K, (b) 308 K and (c) 318 K (pH: 6.0; contact time: 120 min; adsorbent dose: 0.1 g).

The effect of temperature on the removal of MV from aqueous solutions was investigated with the Fe_3O_4-AC composite system. The effect of temperature is shown in Fig. 11.

Thermodynamic parameters were applied to Gibbs free energy ($\Delta G°$), enthalpy ($\Delta H°$) and entropy ($\Delta S°$) and MV adsorption on Fe_3O_4-AC sorbents as thermodynamic [42–46]. The expression of free energy in terms of enthalpy and entropy is given in Eqs. (7)–(9).

$$\Delta G° = \Delta H° - T\Delta S° \quad (7)$$

Here $\Delta G°$ is the change in free energy, kJ/mol; $\Delta H°$ is the enthalpy change, kJ/mol; $\Delta S°$ is the entropy change, J/K mol; T is the absolute temperature (K).

The Gibbs free energy is related to the thermodynamic equilibrium constant K. Eq. (8) is used to calculate the equilibrium constant K.

$$K = \frac{q_e}{C_e} \quad (8)$$

where K is the adsorption equilibrium constant; q_e is the amount of substance retained in the unit mass of the adsorbent (mg/g); C_e is the concentration of dyestuff remaining in solution after adsorption (mg/L).

The standard Gibbs free energy of adsorption is found when K, which is found with the help of the above equation, is replaced in the following equation:

$$\Delta G° = -RT\ln K \quad (9)$$

where K is the adsorption equilibrium constant obtained in adsorption system; $\Delta G°$ is the free energy exchange; R is the universal gas constant (8.314 J/mol K); T is the absolute temperature (K)

When Table 2 is examined, it is seen that all Gibbs free energy values are negative. A negative $\Delta G°$ indicates that adsorption is spontaneous [47]. Furthermore, the decrease in $\Delta G°$ with the increase in temperature shows that MV is more readily adsorbed at higher temperatures [45]. The negative $\Delta H°$ value obtained in our study shows that the adsorption process is exothermic. Standard entropy values ($\Delta S°$) are negative at all temperatures. A negative $\Delta S°$ value indicates no structural change between the adsorbent and the dye.

3.7. Analysis of kinetic study results

In order to determine the kinetics of adsorption process, pseudo-first-order and pseudo-second-order kinetic

Table 2
Thermodynamic parameters of Methyl violet adsorption

Sample	T (K)	$\Delta G°$ (kJ/mol)	$\Delta H°$ (kJ/mol)	$\Delta S°$ (J/mol)
Fe_3O_4-AC	298	–8.23		
Fe_3O_4-AC	308	–6.35	–59.43	–0.172
Fe_3O_4-AC	318	–4.81		

Table 1
Freundlich and Langmuir isotherm constants for Methyl violet adsorption

Temperature (K)	Sample	Langmuir isotherms			Freundlich isotherms		
		q_m (mg/g)	b (L/mg)	R^2	K_f	n (L/mg)	R^2
298	Fe_3O_4-AC	156.25	0.37	0.98	40.52	1.91	0.84
308	Fe_3O_4-AC	155.84	0.19	0.95	24.18	1.69	0.90
318	Fe_3O_4-AC	136.98	0.21	0.96	17.85	1.89	0.85

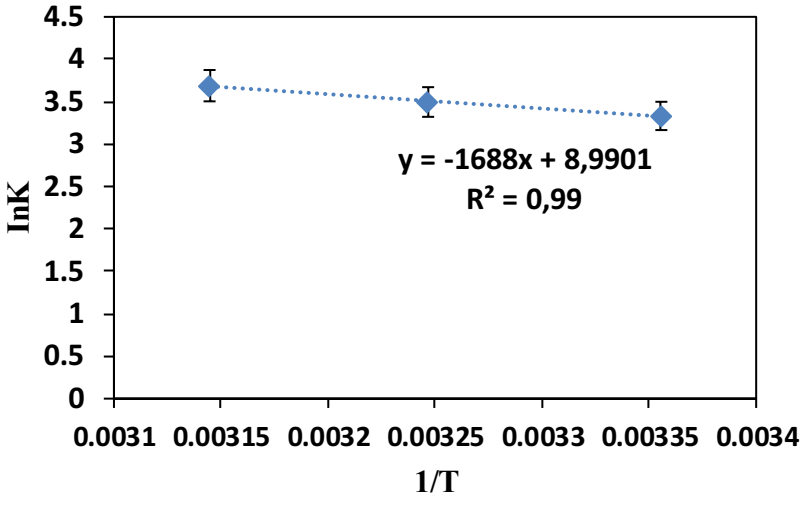

Fig. 11. 1/T graph against lnK_d.

models were applied. Adsorption kinetics Fe_3O_4 coated acorn were analyzed using pseudo first order and pseudo-second-order.

The kinetic mechanism of MV adsorption on Fe_3O_4-AC adsorbent was determined with the help of Pseudo first order and pseudo-second-order kinetic models. The adsorption of Fe_3O_4-AC with three different initial concentrations (50–100–150 mg/L) of MV, correlation coefficient and first order adsorption rate constants were calculated from the slope of the line obtained from the graph of $\log(q_e - q_t)$ vs. time values. Figs. 12 and 13 show pseudo-first and second-order kinetic models. The correlation coefficient (>0.80) obtained from the calculations in Table 3 was found to be suitable for defining the kinetic mechanism of the adsorption process

Table 3 shows the results from first and second-order kinetic modeling. A very high correlation coefficient was obtained for the pseudo-second-kinetic model. In this model, q_e values obtained from experimental data and

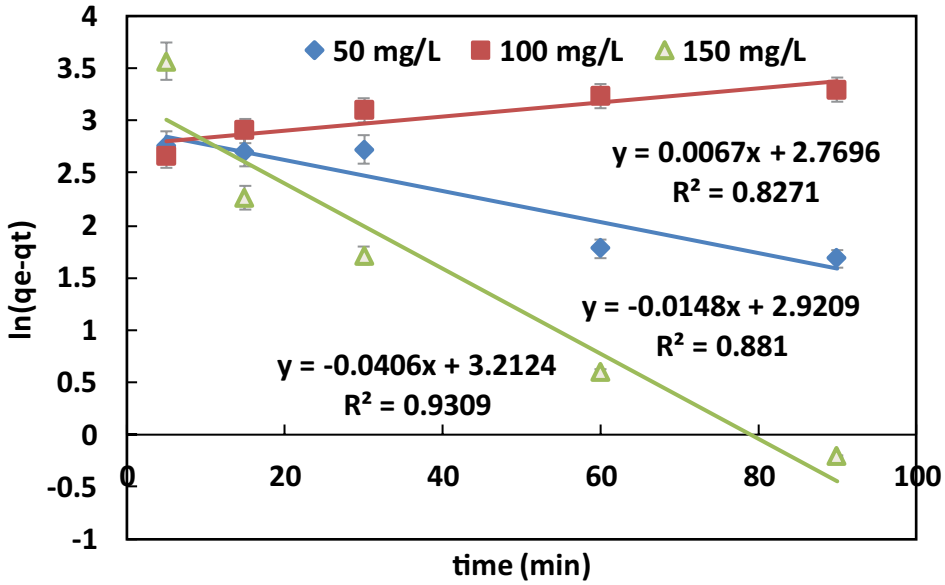

Fig. 12. Pseudo-first-order kinetics of the adsorption of MV onto Fe_3O_4-AC (MV concentration 50, 100 and 150 mg/L; dosage 0.1 g; pH = 6.0).

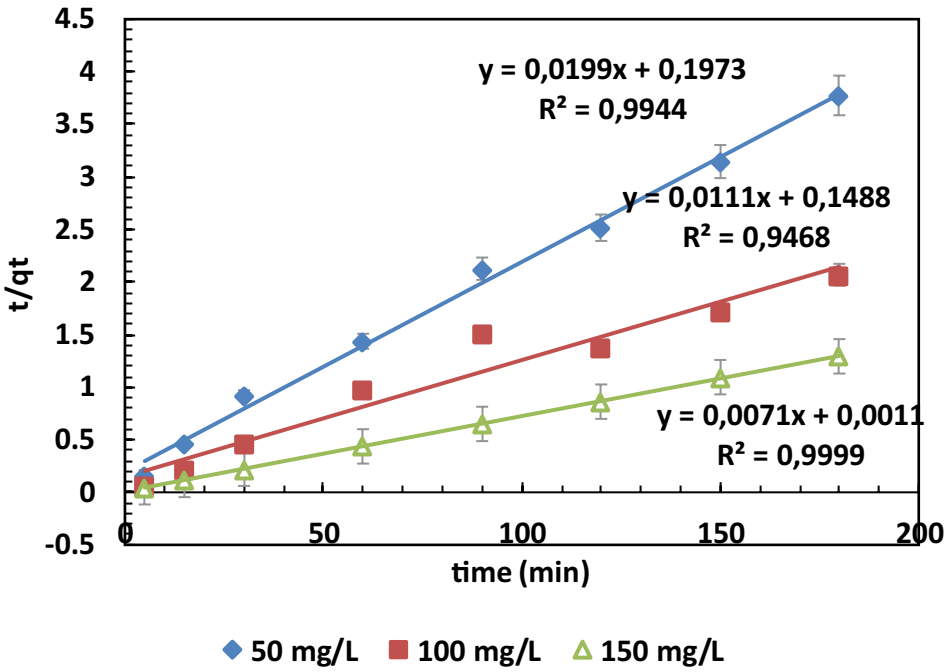

Fig. 13. Pseudo-second-order kinetics of the adsorption of MV onto Fe_3O_4-AC (MV concentration 50, 100 and 150 mg/L; dosage 0.1 g; pH = 6.0).

Table 3
Parameters of the pseudo-first-order and the pseudo-second-order for Methyl violet adsorption

		Pseudo-first-order			Pseudo-second-order		
C_0 (mg/L)	$q_{e,exp}$	$k_1 \times 10$ (dak^{-1})	$q_{e,cal}$ (mg/g)	R^2	$k_2 \times 10^3$ (g/mg h)	$q_{e,cal}$ (mg/g)	R^2
100	48.02	0.015	15.95	0.83	0.07	90.90	0.94
150	139.15	0.07	19.75	0.85	0.65	140.85	1.00

theoretically found q_e values were found to be very close. According to these results, we can say that our study fits pseudo-second-kinetic model.

3.8. Desorption

Desorption application is very important to remove the MV impregnated on magnetic nanoparticles and to clarify the accuracy of adsorption study data. In the desorption study, firstly, five different NaOH solutions between 0.1–0.5 M were used. Desorption efficiency was calculated as 87.49%, 92.23%, 93.14%, 94.48% and 95.45%, respectively. The best desorption efficiency was observed at 0.5 M NaOH M and the cycle work was continued at this concentration. The results of the adsorption-desorption cycle obtained from the adsorption of MV dye on the Fe_3O_4-AC adsorbent are given in Fig. 14.

The amount of MV adsorbed to the Fe_3O_4-AC sorbent was 93.28% removal after the first three reuse cycles. After the sixth cycle, it decreased to 61.28% and stabilized in this way. It resulted in a reduction of approximately 39% during desorption between 1–7 cycles. When the results obtained were examined, a recovery rate of 61.28% was achieved. These results show the feasibility of Fe_3O_4-AC sorbent in terms of reusability.

3.9. Modeling of MV adsorption on Fe_3O_4-AC with ANN

The R value used in artificial intelligence studies is available in graphs containing experimental and predictive data. The R^2 value is a statistical method used to measure the relationship of a variable to two or more variables, or the linear relationship or degree between two variables. The neuron was used in the hidden layer, and it was determined by trial-and-error method according to the obtained R^2 value. In this study, a three-layer feed forward back propagation neural network (5:15:1) was used for modeling the adsorption process. After the input variables are defined as entering the system, the graphic given by the program is presented in Fig. 15.

When Fig. 15 is examined, the graphs consist of three indicators: Data, Fit and $Y = T$. While there are experimental data used in network training on the X-axis, there are estimated values on the Y-axis. The foot line shows the relationship between input and predicted value. The $Y = T$ line is the true value, and the estimated value is equal, that is, the target line. Data are model estimation values obtained with ANN. The correlation obtained from the training data for the ANN model optimized structure is shown in Fig. 15a. As can be seen in Fig. 15b and c, it performed relatively well in validation and testing, although distributed in some data. The regression coefficient was determined as 99% for

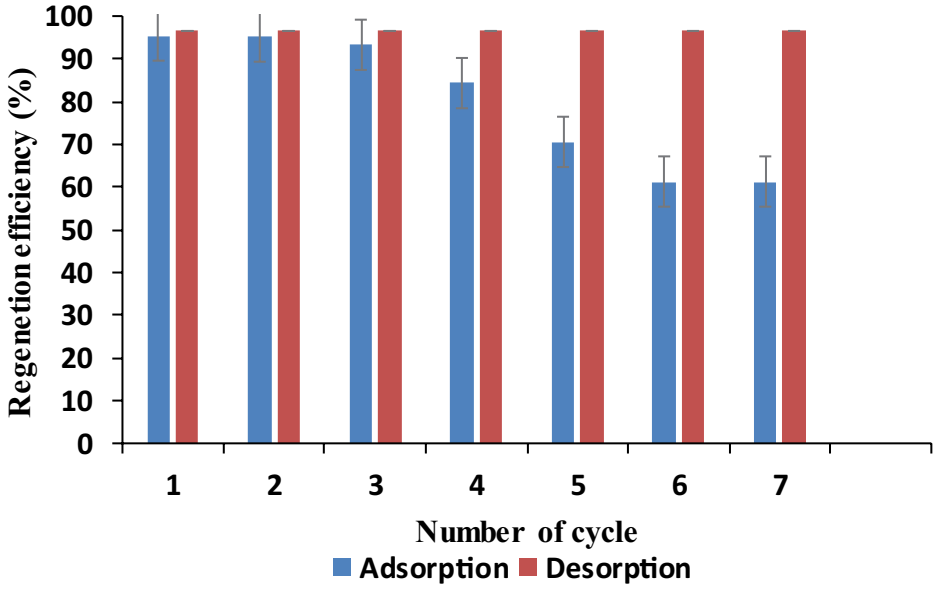

Fig. 14. Recycling performance of the prepared Fe_3O_4-AC adsorbent (temperature: 298 K; adsorbent dosage: 0.1 g/100 mL; contact time: 120 min; pH: 6.0).

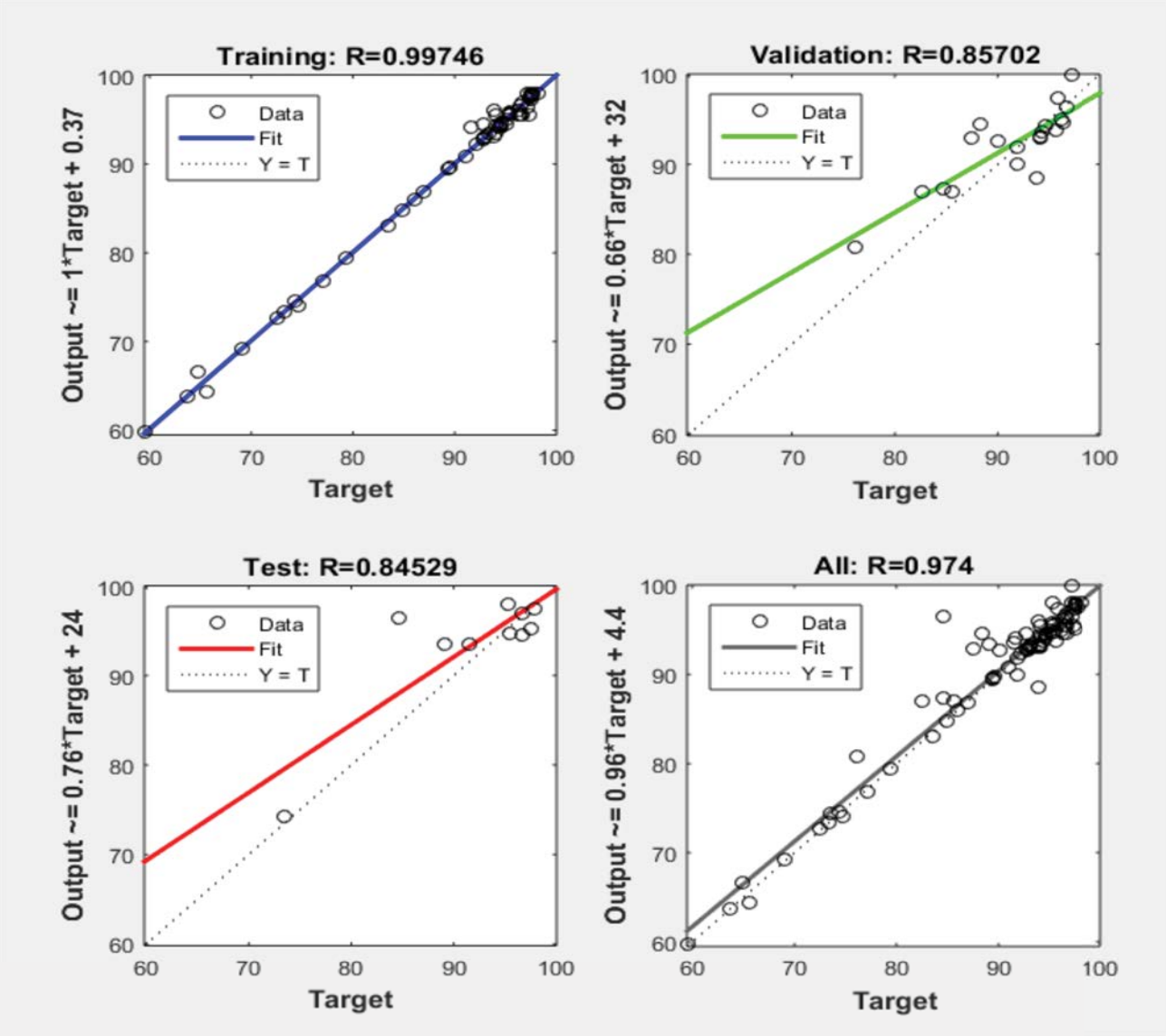

Fig. 15. ANN predictive model graph.

training, 85% for verification, and 84% for testing for training, validation and testing phases. Fig. 15d shows the bulk adsorption experimental data set. The optimal topology for the adsorption of MV on Fe_3O_4-AC was determined with R^2 and MSE values of 0.97 and 0.045, respectively. The complex relationship between the high correlation coefficient obtained and the ANN input–output, namely the number of hidden layers and the number of processing elements in the hidden layer, is determined and the closest network architecture to the desired values is determined and the relationship between input–output variables is well defined. High accuracy estimation emerged between experimental and calculated values [48].

The comparison of the adsorption capacity of the MV we used in our study with different adsorbents is given in Table 4 [25,42–46].

When Table 4 is examined, the maximum adsorption capacity found in the MV removal studies in the literature we give is lower than the value in our study. While the maximum adsorption capacity was between 9.58 and 153.85 mg/g in other studies, this value was found to be 156.25 mg/g in our study. This result indicates that MV removal with Fe_3O_4-AC adsorbent was successful.

4. Conclusions

In this study, AC obtained from acorns and Fe_3O_4-AC were synthesized and its effectiveness in MV removal from aqueous solutions was investigated. Characterization of AC, Fe_3O_4-AC obtained from acorn bark before and after adsorption was performed by FTIR, SEM/EDS and XRD analyses. Maximum adsorption capacity with Langmuir isotherm was found to be 298 K, contact time of 120 min and 156.25 mg/g at 6 pH. The pseudo-second-order kinetic model had a better fit with the best correlation to the kinetic data. A negative value of $\Delta H°$ indicates that the adsorption

Table 4
Comparison of the adsorption capacity of Methyl violet with different adsorbents

Adsorbent	pH	Contact time (min)	Adsorption Capacity (mg g^{-1})	Reference
Moroccan pyrophyllite	6.8	120	9.58	[28]
Sepiolite	6–7	180	10.24	[29]
ACSO/Fe_3O_4	7	50	59.88	[30]
HNT-Fe_3O_4	7	180	20.04	[31]
ACSO	7	50	29.89	[30]
Untreated almond shell	8	40	114	[32]
Activated almond shell	8	40	123	[32]
Z	7	150	135.13	[13]
Z-Fe_3O_4	7	150	153.85	[13]
Fe_3O_4-AC	6	180	156.25	This study

for the sorbent is exothermic. A negative value of $\Delta S°$ indicates that there is no structural change between the adsorbent and the dyestuff. For the reusability of the adsorbent, Fe_3O_4-AC MV adsorption and desorption process was performed in 7 consecutive cycles, and it was seen that it had a reusable potential with a removal value of 61.28% at the end of 7 cycles. At the last stage of the study, the experimental values were fitted with ANN model to estimate their accuracy. With R^2 values higher than the results obtained. It has been observed that the ANN model is a good estimation tool for the system. When the data obtained in this study are examined, it is seen that Fe_3O_4-AC adsorbent is promising in terms of low cost and easy accessibility.

References

[1] A.K. Prajapati, M.K. Mondal, Comprehensive kinetic and mass transfer modeling for methylene blue dye adsorption onto CuO nanoparticles loaded on nanoporous activated carbon prepared from waste coconut shell, J. Mol. Liq., 307 (2020) 112949, doi: 10.1016/j.molliq.2020.112949.

[2] H. Altundag, E. Bina, E. Altıntıg, The levels of trace elements in honey and molasses samples that were determined by ICP-OES after microwave digestion method, Biol. Trace Elem. Res., 170 (2016) 508–514.

[3] P. Arabkhani, A. Asfaram, M. Ateia, Easy-to-prepare graphene oxide/sodium montmorillonite polymer nanocomposite with enhanced adsorption performance, J. Water Process Eng., 38 (2020) 101651, doi: 10.1016/j.jwpe.2020.101651.

[4] C.-G. Tsai, W.J. Tseng, Preparation of TiN–TiO_2 composite nanoparticles for organic dye adsorption and photocatalysis, Ceram. Int., 46 (2020) 14529–14535.

[5] T.V.N. Padmesh, K. Vijayaraghavan, G. Sekaran, M. Velan, Biosorption of Acid Blue 15 using fresh water macroalga *Azolla filiculoides*: batch and column studies, Dyes Pigm., 71 (2006) 77–82.

[6] P. Arabkhani, H. Javadian, A. Asfaram, M. Ateia, Decorating graphene oxide with zeolitic imidazolate framework (ZIF-8) and pseudo-boehmite offers ultra-high adsorption capacity of diclofenac in hospital effluents, Chemosphere, 271 (2021) 129610, doi: 10.1016/j.chemosphere.2021.129610.

[7] S.A. Ong, L.N. Ho, Y.S. Wong, A. Zainuddin, Adsorption behavior of cationic and anionic dyes onto acid treated coconut coir, Sep. Sci. Technol., 48 (2013) 2125–2131.

[8] L. Bulgaria, L.B. Escudero, O.S. Bello, M. Iqbal, J. Nisar, K.A. Adegoke, F. Alakhras, M. Kornaros, I. Anastopoulas, The utilization of leaf-based adsorbents for dyes removal: a review, J. Mol. Liq., 276 (2019) 728–747.

[9] E. Altintig, S. Kirkil, Preparation and properties of Ag-coated activated carbon nanocomposites produced from wild chestnut shell by $ZnCl_2$ activation, J. Taiwan Inst. Chem. Eng., 63 (2016) 180–188.

[10] I. Ali, New generation adsorbents for water treatment, Chem. Rev., 112 (2012) 5073–5091.

[11] H.N. Tran, P.V. Viet, H.-P. Chao, Surfactant modified zeolite as amphiphilic and dual-electronic adsorbent for removal of cationic and oxyanionic metal ions and organic compounds, Ecotoxicol. Environ. Saf., 147 (2018) 55–63.

[12] I. Safarik, R. Angelova, E. Baldikova, K. Pospiskova, M. Safarikova, *Leptothrix* sp. sheaths modified with iron oxide particles: magnetically responsive, high aspect ratio functional material, Mater. Sci. Eng., C, 71 (2017) 1342–1346.

[13] S. Cheng, L. Zhang, A. Ma, H. Xia, J. Peng, C. Li, J. Shu, Comparison of activated carbon and iron/cerium modified activated carbon to remove methylene blue from wastewater, J. Environ. Sci., 65 (2018) 92–102.

[14] Z.A. Al-Othman, R. Ali, Mu. Naushad, Hexavalent chromium removal from aqueous medium by activated carbon prepared from peanut shell: adsorption kinetics, equilibrium and thermodynamic studies, Chem. Eng. J., 184 (2012) 238–247.

[15] R. Ranjith, P.S. Rajam, Removal of cationic dyes from aqueous solution by adsorption on mesoporous TiO_2-SiO_2 nanocomposite, J. Nanosci. Technol., 3 (2017) 273–280.

[16] S. Agarwal, I. Tyagi, V.K. Gupta, A.R. Bagheri, M. Ghadei, A. Asfaram, S. Hajati, A.A. Bazrafshan, Rapid adsorption of ternary dye pollutants onto copper(I) oxide nanoparticle loaded on AC: experimental optimization via response surface methodology, J. Chem. Eng., 4 (2016) 1769–1779.

[17] E.A. Dil, M. Ghaedi, A. Asfaram, F. Mehrabi. Application of modificated magnetic nanomaterial for optimization of ultrasound-enhanced removal of Pb^{2+} ions from aqueous solution under experimental design: investigation of kinetic and isotherm, Ultrason. Sonochem., 36 (2017) 409–419.

[18] M. Ghasemi, S. Mashhadi, J. Azimi-Amin, Fe_3O_4/AC nanocomposite as a novel nano adsorbent for effective removal of cationic dye: process optimization based on Taguchi design method, kinetics, equilibrium and thermodynamics, J. Water Environ. Nanotechnol., 3 (2018) 321–336.

[19] L.C.A. Oliveira, R.V.R.A. Rios, J.D. Fabris, K. Sapag, V.K. Garg, R.M. Lago, Clay-iron oxide magnetic composites for the adsorption of contaminants in water, Appl. Clay Sci., 22 (2003) 169–177.

[20] D. Salari, N. Daneshvar, F. Aghazadeh, A.R. Khataee, Application of artificial neural networks for modeling of the treatment of wastewater contaminated with methyl tert-butyl ether (MTBE) by UV/H_2O_2 process, J. Hazard. Mater., 125 (2005) 205–210.

[21] A. Alebouyeh, A.M.B. Kasiri, M.E. Olya, H. Aleboyeh, Prediction of azo dye decolorization by UV/H_2O_2 using artificial neural networks, Dyes Pigm., 77 (2008) 288–294.

[22] M. Zarei, N. Djafarzadeh, L. Khadir, Removal of direct blue 129 from aqueous medium using surfactant-modified zeolite:

a neural network modelling, Environ. Health Eng. Manage. J., 5 (2018) 101–113.
[23] S. Coruh, E. Kılıç, F. Geyikci, Prediction of adsorption efficiency for the removal malachite green and acid blue 161 dyes by waste marble dust using ANN, Global Nest J., 16 (2014) 676–689.
[24] J.N. Miller, J.C. Miller, Statistics and Chemometrics for Analytical Chemistry, Harlow, England, Pearson Education, 2005.
[25] E. Altintig, A. Alsancak, H. Karaca, D. Angın, H. Altundag, The comparison of natural and magnetically modified zeolites as an adsorbent in Methyl violet removal from aqueous solutions, Chem. Eng. Commun., (2021), doi: 10.1080/00986445.2021.1874368.
[26] M. Sadrzadeh, T. Mohammadi, J. Ivakpour, N. Kasiri, Separation of lead ions from wastewater using electrodialysis: comparing mathematical and neural network modeling, Chem. Eng. J., 144 (2008) 431–441.
[27] L. Ai, C. Zhang, F. Liao, Y. Wang, M. Li, L. Meng, J. Jiang, Removal of methylene blue from aqueous solution with magnetite loaded multi-wall carbon nanotube: kinetic, isotherm and mechanism analysis, J. Hazard. Mater., 198 (2011) 282–290.
[28] E. Altıntıg, H. Altundag, M. Tuzen, A. Sarı, Effective removal of methylene blue from aqueous solutions using magnetic loaded activated carbon as novel adsorbent, Chem. Eng. Res. Des., 122 (2017) 151–163.
[29] N.S. Maurya, A.K. Mittal, P. Cornel, E. Rother, Biosorption of dyes using dead macro fungi: effect of dye structure, ionic strength and pH, Bioresour. Technol., 97 (2006) 512–521.
[30] J. Xu, X. Rong, T. Chi, M. Wang, Y. Wang, D. Yang, F. Qiu, Preparation, characterization of UV-curable waterborne polyurethane-acrylate and the application in metal iron surface protection, J. Appl. Polym. Sci., 130 (2013) 3142–3152.
[31] F. Sadeghfar, M. Ghaedi, A. Asfaram, R. Jannesar, H. Javadian, V. Pezeshkpour, Polyvinyl alcohol/Fe_3O_4@carbon nanotubes nanocomposite: electrochemical-assisted synthesis, physico-chemical characterization, optical properties, cytotoxicity effects and ultrasound-assisted treatment of aqueous based organic compound, J. Ind. Eng. Chem., 65 (2018) 349–362.
[32] J. Xu, W. Ji, Characterization of ZnS nanoparticles prepared by new route, J. Mater. Sci., 18 (1999) 115–117.
[33] L.Y. Hsu, H. Teng, Influence of different chemical reagents on the preparation of activated carbon from bituminous coal, Fuel Process. Technol., 64 (2000) 155–166.
[34] H. Deng, G. Li, H. Yang, J. Tang, Preparation of activated carbons from cotton stalk by microwave assisted KOH and K_2CO_3 activation, Chem. Eng. J., 163 (2010) 373–381.
[35] H. Esmaeili, S. Tamjidi, Ultrasonic-assisted synthesis of natural clay/Fe_3O_4/graphene oxide for enhance removal of Cr(VI) from aqueous media, Environ. Sci. Pollut. Res., 27 (2020) 31652–31664.
[36] X. Zhao, Y. Shi, T. Wang, Y. Cai, G. Jiang, Preparation of silica-magnetite nanoparticle mixed hemimicelle sorbents for extraction of several typical phenolic compounds from environmental water samples, J. Chromatogr. A, 1188 (2008) 140–147.
[37] S.S. Gupta, G.B. Krishna, Kinetics of adsorption of metal ions on inorganic materials, a review, Adv. Colloid Interface Sci., 162 (2011) 39–58.
[38] X. Xiao, S. Luo, G. Zeng, W. Wei, Y. Wan, L. Chen, H. Gou, Z. Cao, L. Yang, J. Chen, Q. Xi, Biosorption of cadmium by endophytic fungus (EF) *Microshaeropsis* sp. LSE10 isolated from cadmium hyperaccumulator *Solanum nigrum* L, Biosesour. Technol., 101 (2009) 1668–1674.
[39] A. Khaled, A. El Nemr, A. El-Sikaily, O. Abdelwahab, Treatment of artificial textile dye effluent containing Direct Yellow 12 by orange peel carbon, Desal. Water Treat., 238 (2009) 210–232.
[40] E. Altıntıg, M. Daglar, H. Altundag, Removal of methylene blue with nanomagnetic coated wild chestnut shells: thermodynamic, kinetic, isotherm and mechanism studies, Desal. Water Treat., 207 (2020) 398–409.
[41] A.M.M. Vargas, A.L. Cazetta, M.H. Kunita, T.L. Silva, V.C. Almeida, Adsorption of methylene blue on activated carbon produced from flamboyant pods (*Delonix regia*): study of adsorption isotherms and kinetic models, Chem. Eng. J., 168 (2011) 722–730.
[42] Y. Miyah, A. Lahrichi, M. Idrissi, S. Boujraf, H. Taouda, F. Zerrouq, Assessment of adsorption kinetics for removal potential of Crystal Violet dye from aqueous solutions using Moroccan pyrophyllite, J. Assoc. Arab Univ. Basic Appl. Sci., 23 (2017) 20–28.
[43] M. Dogan, Y. Ozdemir, M. Alkan, Adsorption of cationic dyes from aqueous solutions by sepiolite, Microporous Mesoporous Mater., 96 (2006) 419–427.
[44] R. Foroutana, R. Mohammadi, J. Razeghib, B. Ramavandi, Performance of algal activated carbon/Fe_3O_4 magnetic composite for cationic dyes removal from aqueous solutions, Algal Res., 40 (2019) 1–12.
[45] L.R. Bonetto, F. Ferrarini, D.C. Marco, J.S. Crespo, Removal of Methyl violet 2B dye from aqueous solution using a magnetic composite as an adsorbent, J. Water Process Eng., 6 (2015) 11–20.
[46] M. Ishaq, F. Javed, I. Amad, H. Ullah, F. Hadi, S. Sultan, Adsorption of crystal violet dye from aqueous solutions onto low-cost untreated and NaOH treated almond shell, Iran. J. Chem. Chem. Eng., 35 (2016) 97–106.
[47] D. Sara, K.S. Tushar, Removal of anionic dye Congo red from aqueous solution by raw pine and acid-treated pinecone powder as adsorbent: equilibrium, thermodynamic, kinetics, mechanism and process design, Water Res., 46 (2012) 1933–1946.
[48] EA. Dil, M. Ghaedia, A. Asfaram, F. Mehrabi, F. Sadeghfar, Efficient adsorption of Azure B onto CNTs/Zn:ZnO@Ni_2P-NCs from aqueous solution in the presence of ultrasound wave based on multivariate optimization, J. Ind. Eng. Chem., 74 (2019) 55–62.